Nonisothermal Crystallization Kinetics of Poly(ethylene terephthalate)/Antimony-Doped Tin Oxide Nanocomposites

Xiaolei Chen,[1,2] Chunzhong Li,[1] Wei Shao,[1] Tianxi Liu,[3] Lumin Wang[2]

[1]*Key Laboratory for Ultrafine Materials of the Ministry of Education, School of Materials Science and Engineering, East China University of Science and Technology, Shanghai 200237, People's Republic of China*
[2]*Key and Open Laboratory of Marine and Estuarine Fisheries of the Ministry of Agriculture, East China Sea Fisheries Research Institute, Chinese Academy of Fishery Sciences (CAFS), Shanghai 200090, People's Republic of China*
[3]*Laboratory of Advanced Materials, Fudan University, Shanghai 200433, People's Republic of China*

Received 22 January 2007; accepted 22 January 2008
DOI 10.1002/app.28069
Published online 6 June 2008 in Wiley InterScience (www.interscience.wiley.com).

ABSTRACT: Poly(ethylene terephthalate) (PET)/antimony-doped tin oxide (ATO) nanocomposites were prepared by *in situ* polymerization. The nonisothermal crystallization behaviors of neat PET and PET/ATO nanocomposites were investigated with differential scanning calorimetry. The nonisothermal crystallization data were analyzed with the Avrami analysis modified by Jeziorny, the Ozawa method, and a method developed by Liu et al. The modified Avrami equation could describe only the primary stage of nonisothermal crystallization of PET and PET/ATO nanocomposites. The Ozawa analysis, when applied to the polymer systems studied here, failed to describe their nonisothermal crystallization behavior. The kinetic method developed by Liu et al. was successful in describing the nonisothermal crystallization of neat PET and PET/ATO nanocomposites. According to the Kissinger equation, the activation energies were determined to be −205.3, −220.0, and −243.7 kJ/mol for neat PET and 99/1 and 95/5 PET/ATO nanocomposites, respectively. © 2008 Wiley Periodicals, Inc. J Appl Polym Sci 109: 3753–3762, 2008

Key words: crystallization; nanocomposites; nanotechnology; polyesters

INTRODUCTION

Nanocomposites have attracted a great deal of interest over the past years because of the potentially superior properties that these materials can exhibit with respect to conventional composites. Numerous studies have shown that a very low percentage of nanoparticles can lead to a significant enhancement of many properties for polymer matrices, such as stiffness and strength,[1,2] flame retardancy,[3,4] gas barrier properties,[5,6] ionic conductivity,[7,8] and thermal stability.[9]

Poly(ethylene terephthalate) (PET) is a widely used engineering polymer. The specific resistance of PET is more than 10^{14} Ω cm because of a lack of polar groups, and the problem with static restricts its further applications. At present, antistatic PET nanocomposites have been prepared mainly by the addition of carbon black or carbon nanotubes.[10,11] However, the dyeing behavior of PET with carbon black or carbon nanotubes is unsatisfactory. Therefore, in our work, antimony-doped tin oxide (ATO) nanoparticles were introduced into PET to improve its antistatic property. ATO exhibits both optical transparency to visible radiation and high electrical conductivity. ATO has been the focus of intensive studies because of its high-temperature, chemical, and mechanical stability.[12] At a low antimony doping level, the conductivity of ATO is greatly increased in comparison with pure tin oxide and can be varied easily by changes in the antinomy doping level.[13] When used as an antistatic agent, ATO shows better performance than the currently used carbon blacks, metallic pigments, and organic polymer binders.[14] A novel finishing agent containing an ultrafine conductive ATO powder was prepared by Wu et al.[15] and used for an antistatic treatment of PET fabric. The surface resistance of the PET fabric treated by the novel finishing agent could be reduced from 10^{12} to 10^{10} Ω.

Correspondence to: C. Li (czli@ecust.edu.cn).
Contract grant sponsor: National Natural Science Foundation of China; contract grant number: 20236020.
Contract grant sponsor: Shanghai Municipal Science and Technology Commission; contract grant numbers: 04DZ14002, 04DZ05622, 05DZ22302 and 045211021.
Contract grant sponsor: Sepacial Project for Shanghai Nanotechnology; contract grant numbers: 0452nm001, 0452nm047 and 0552nm001.
Contract grant sponsor: 973 Program; contract grant number: 2004CB719500.

TABLE I
Characteristics of the ATO Sample

Sample	Brunauer–Emmett–Teller surface area (m^2/g)	Average particle size (nm)	Volume resistivity (Ω cm)
ATO	65	20	1–5

The effect of the addition of ATO on the structural, thermal, electrical, and mechanical properties of PET is under investigation in our laboratory. The nonisothermal crystallization behavior of PET/clay nanocomposites was studied by Wang et al.[16] They reported that the crystallization rate of PET/clay nanocomposites was faster than that of PET at a given cooling rate, and the absolute value of the activation energy for PET was lower than that of PET/clay nanocomposites. The study of the nonisothermal crystallization of composites is of great technological importance because most composites and polymer blends are processed under nonisothermal conditions. As PET is a semicrystalline polymer and its mechanical and thermal properties are strongly dependent on the processing conditions, the analysis of the nonisothermal crystallization kinetics of PET and PET/ATO nanocomposites was carried out with differential scanning calorimetry (DSC) in this study.

EXPERIMENTAL

Materials

The details of preparing ATO nanoparticles by a chemical coprecipitation method were described previously,[17] and their characteristics are listed in Table I. Ethylene glycol (EG), antimony acetate (as a catalyst), antimony trioxide (as a catalyst), and terephthalic acid (TPA) were kindly supplied by the Shanghai Chemical Fiber Institute (Shanghai, China). A silane coupling agent, y-methacryloxypropyl trimethoxysilane (A-174), was supplied by Shanghai YaoHua Chemical Plant (Shanghai, China). The chemical structure of A-174 is expressed as $CH_2{=}C(CH_3)CO_2\text{-}(CH_2)_3Si(OCH_3)_3$.

The nanocomposites were synthesized with a 2-L reactor (fabricated by the Shanghai Chemical Fiber Institute). The ATO nanoparticles were modified by silane coupling agent A-174 and dispersed in a solution of EG by high-speed ball milling.[18] As an example, the preparation of the nanocomposite containing 1 wt % ATO is described here. In the 2-L reactor, 403 g of EG (with 12.7 g of modified ATO), 830 g of TPA, 0.017 g of antimony acetate, and 0.248 g of antimony trioxide were placed. This mixture was agitated at 30 rpm before heating and then heated in a nitrogen atmosphere from room temperature to 260–270°C under a pressure of 0.15 MPa for esterification. After complete esterification, the pressure was slowly reduced to air pressure to release the water generated during the esterification. Afterward, the polymerization was carried out at 275–280°C for about 120–150 min, and the pressure of polymerization was gradually reduced up to 70 Pa by vacuumization. Finally, the polymer melt was extruded through an orifice at the N_2 pressure of 0.15 MPa and cooled with water. The neat PET and PET/ATO nanocomposites (with ATO weight contents of 1 and 5%) were fabricated with the same process.

The product was dried *in vacuo* at 80°C for 24 h and then was dissolved in solvents of 50/50 (w/w) phenol/1,1,2,2-tetrachloroethane (TCE). The solution viscosity was measured with an Ubbelohde viscome-

TABLE II
Characteristic Data of Nonisothermal Crystallization Exotherms for Various Samples

Sample	η_{inh}[a]	Φ (°C/min)	T_p (°C)	$t_{1/2}$ (min)	ΔH_c (J/g)	X_c (%)
Neat PET	0.645	2.5	201.18	2.96	44.63	31.88
		5	195.23	1.96	36.37	25.98
		10	187.36	1.34	35.76	25.54
		20	182.98	0.71	33.74	24.10
1/99 ATO/PET	0.685	2.5	206.38	2.61	53.06	37.90
		5	200.86	1.90	43.50	31.07
		10	193.65	1.22	43.43	31.02
		20	188.83	0.71	39.12	27.94
5/95 ATO/PET	0.725	2.5	204.64	2.39	45.04	32.17
		5	201.56	1.36	38.66	27.61
		10	194.32	1.00	37.88	27.06
		20	189.43	0.53	33.44	23.89

[a] Inherent viscosity measured at 30°C with 0.1 g/100 mL solutions in a phenol/TCE (w/w) mixture.

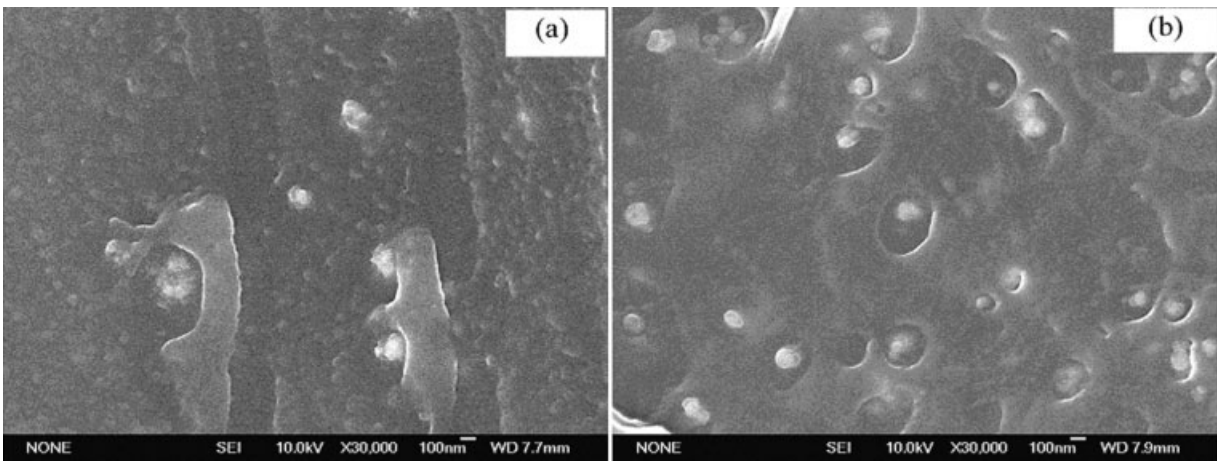

Figure 1 FESEM micrographs of PET/ATO nanocomposites: (a) 99/1 PET/ATO and (b) 97.5/2.5 PET/ATO.

ter. The limiting viscosity numbers of the neat PET and PET/ATO nanocomposites are listed in Table II.

Field emission scanning electron microscopy (FESEM)

The morphologies of the fractured surfaces of PET/ATO nanocomposites were investigated with FESEM with a JEOL (Tokyo, Japan) JEM-6700F electron microscope operated at 5 kV. The fractured surfaces of the samples were sputter-coated with a thin layer of gold.

DSC

Nonisothermal crystallization kinetics were determined with a Netzsch model PC200 differential scanning calorimeter (Selb, Germany). The instrument was calibrated with high-purity indium and zinc. All DSC measurements were performed under a dry nitrogen flow, and an empty aluminum pan was used as a reference. The samples were heated quickly (at 50°C/min) to 300°C for 10 min to ensure total relaxation of the samples and to eliminate the influence of the thermal history. Then, the melts were rapidly cooled to 100°C at different cooling rates of 2.5, 5, 10, and 20°C/min for the nonisothermal crystallization process (shown later in Fig. 2). The exothermic curves of heat flow as a function of time were recorded and investigated.

RESULTS AND DISCUSSION

Morphological analysis of the PET/ATO nanocomposites

It is well known that the conformation and properties of nanocomposites generally depend on the shape, size, and dispersion in the matrix of the nanoparticles. Figure 1 shows scanning electron microscopy images of the fractured surfaces of PET/ATO nanocomposites with different ATO contents. The ATO nanoparticles were well dispersed in the polymer matrix when the concentration of the filler was low [Fig. 1(a)]. The dispersion was also homogeneous, and the sizes of the ATO aggregates did not increase with high concentrations of the filler [Fig. 1(b)]. In addition, for the nanocomposites, ATO was still well dispersed in the polymer matrix after spinning.[19] The ATO nanoparticles used here were first modified by silane coupling agent A-174 and dispersed in the solution of EG by high-speed ball milling. The PET/ATO nanocomposites were prepared by means of esterification and condensation reactions of TPA and EG in the presence of ATO nanoparticles. The ATO nanoparticles modified with the silane coupling agent could be well dispersed into EG because of the incorporation of the coupling agent with the surface of the ATO particles, and the steric effect from the presence of the silane coupling agent was helpful for preventing particle agglomeration in EG.[18] Meanwhile, TPA was compatible with the EG solution above 200°C. Finally, a good dispersion of ATO in the polymer matrix was obtained, as shown in Figure 1. The silane coupling agent was physically bonded with ATO because of the few hydroxyl groups on the surface of ATO. During the *in situ* polymerization, the silane coupling agent decomposed (the decomposition temperature of the silane coupling agent A-174 is ca. 255°C) and had little influence on the electrical property of ATO. The ATO nanoparticles could not be monodispersed in the PET matrix and were in the form of an agglomerate with a diameter of 80–100 nm, as shown in Figure 1. The agglomerate had many branched chains that more easily formed a conducting network structure than monodispersed ATO, and the resultant PET/ATO nanocomposites showed a good antistatic property.[19]

Nonisothermal crystallization behavior

Figure 2 shows typical DSC scans of neat PET and PET/ATO nanocomposites cooled from 300°C at various rates. From these curves, the peak crystallization temperature (T_p) and crystallization enthalpy

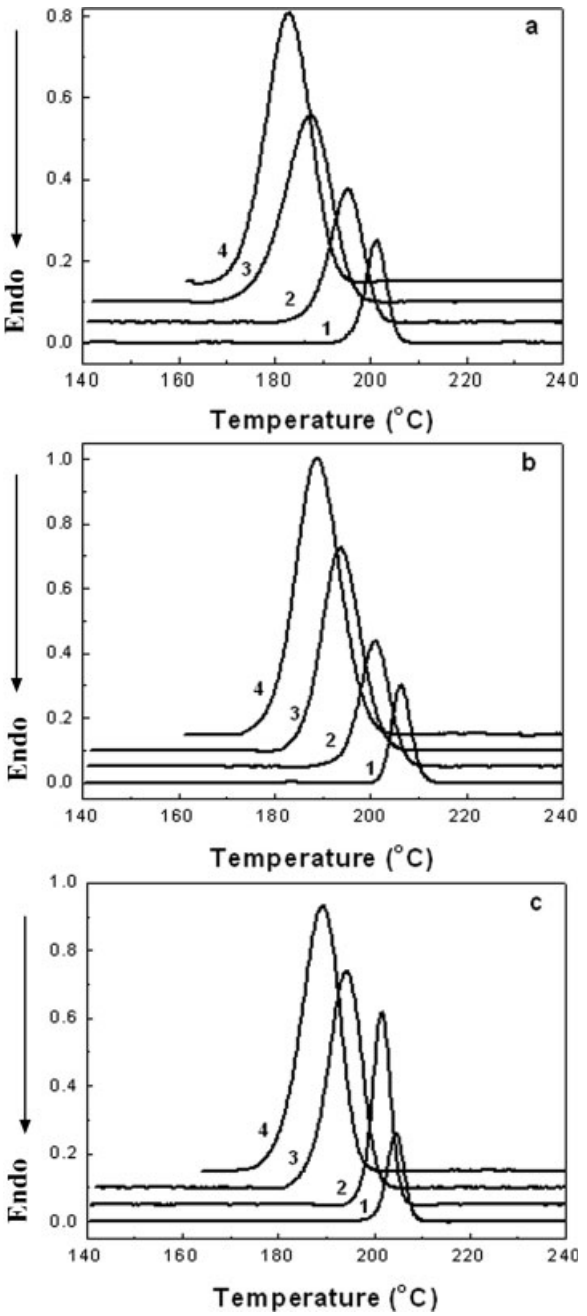

Figure 2 Nonisothermal melt crystallization exotherms of PET and its ATO nanocomposites at cooling rates of (1) 2.5, (2) 5, (3) 10, and (4) 20°C/min: (a) neat PET, (b) 99/1 PET/ATO, and (c) 95/5 PET/ATO.

(ΔH_c) values of all the samples under different cooling rates have been obtained, and they are listed in Table II. Moreover, the degree of crystallinity (X_c) can be calculated from the heat that evolves during crystallization (ΔH_c) with the following relation:

$$X_c(\%) = \frac{\Delta H_c}{(1-b)\Delta H_m} \times 100 \quad (1)$$

where ΔH_m is the heat of fusion for 100% crystalline PET and b is the weight fraction of the filler in the composite. Here, we adopted 140 J/g as the value of ΔH_m.[20] The values of X_c of PET and its nanocomposites, obtained with eq. (1), are summarized in Table II.

From Figure 2 and Table II, it can be seen that T_p steadily decreased with the increase in the cooling rate for each sample, and this indicates that the lower the cooling rate was, the earlier the crystallization occurred. In addition, for a given cooling rate, T_p of neat PET was lower than that of the PET/ATO nanocomposites, and this indicates that ATO acted as a nucleating agent and thus promoted the crystallization of PET for the PET/ATO nanocomposites. However, T_p of the 95/5 PET/ATO nanocomposite was lower than that of the 99/1 PET/ATO nanocomposite with a low cooling rate (2.5°C/min). In general, the overall crystallization process includes nucleation and growth processes. From Table II, it can be seen that the limiting viscosity number of PET increased as the content of ATO increased. According to the Mark–Houwink relationship, $[\eta] = 2.1 \times 10^{-4} M_n^{0.82}$ (where $[\eta]$ is the intrinsic viscosity and M_n is the number-average molecular weight),[21] a larger limiting viscosity number suggests a larger molecular weight. A higher molecular weight results in the molecular mobility decreasing. Thus, T_p of the 95/5 PET/ATO nanocomposite was lower than that of the 99/1 PET/ATO nanocomposite with the cooling rate of 2.5°C/min, and this could be attributed to the fact that their crystallization was under the control of a growth process. That is, it was more difficult for the 95/5 PET/ATO nanocomposite polymer chain to diffuse into the crystalline lattice, and this resulted in lower T_p in comparison with the 99/1 PET/ATO nanocomposite. When the cooling rate was high (≥5°C/min), the crystallization of the PET/ATO nanocomposite was under the control of a nucleation process, and T_p of the nanocomposite increased with the increase in the ATO loadings at a given cooling rate.

The values of X_c in Table II indicate that the addition of ATO to PET resulted in an increase in X_c. For the nonisothermal crystallization of neat PET and its ATO nanocomposites, the values of ΔH_c increased as the cooling rate decreased. Because the absolute degree of crystallization of a sample is equal to the enthalpy for the unit of mass of the sample (ΔH_c) divided by the heat of fusion of a perfect PET crystal, it can be concluded from Table II that the absolute degree of crystallinity for the PET/ATO nanocomposites was higher than that for neat PET.[22] However, X_c of the 95/5 PET/ATO nanocomposite was lower than that of the 99/1 PET/ATO nanocomposite, and this could be attributed to a large number of ATO nanoparticles restricting the mobility of the PET chain. In addition, the 95/5 PET/ATO nanocomposite had a higher molecular weight, and long

polymer chains (high molecular weight) exhibited lower diffusion rates during the crystallization process.

The relative degree of crystallinity as a function of crystallization temperature T [$X(T)$] can be formulated as follows:[23]

$$X(T) = \int_{T_0}^{T} \left(\frac{dH_c}{dT}\right) dT \Big/ \int_{T_0}^{T_\infty} \left(\frac{dH_c}{dT}\right) dT \qquad (2)$$

where T_0 and T_∞ represent the crystallization onset and end temperatures, respectively, and dH_c is the enthalpy of crystallization released in infinitesimal temperature range dT.

Figure 3 shows $X(T)$ for PET and PET/ATO nanocomposites at various cooling rates. The horizontal temperature scale can be transformed into the time domain with the following relationship:

$$t = (T_0 - T)/\Phi \qquad (3)$$

where T is the temperature at crystallization time t and Φ is the cooling rate. The plots of the relative degree of crystallinity as a function of time [$X(t)$] for PET and PET/ATO nanocomposites at different cooling rates are illustrated in Figure 4.

An important parameter that can be taken directly from Figure 4 is the half-time of crystallization ($t_{1/2}$), which is the change in time from the onset of crystallization to the time at which $X(T)$ is 50%. The $t_{1/2}$ values of nonisothermal crystallization for neat PET and PET/ATO nanocomposites are listed in Table II. From Table II, it can be seen that for a given cooling rate, the $t_{1/2}$ values of the nanocomposites were lower than that of neat PET, further indicating that ATO played a nucleating role during the crystallization of PET.

In addition to $t_{1/2}$, other parameters (e.g., the kinetic rate coefficient) are commonly used to characterize the nonisothermal crystallization kinetics of polymers. The crystallization kinetics of polymers constitute a complicated process that involves two important steps, that is, the diffusion of crystallizable chains to the crystal front and nucleation. As the diffusive molecule reaches the crystal boundary, it must form a stable nucleus, and this is followed by the growth of the crystallites. Thus, the crystallization processes are affected, to a certain degree, by the thermodynamic conditions under which the crystallization takes place, by the molecular characteristics, and by the interaction between the polymer and filler. Therefore, the determination of the kinetic parameters enables us to better understand how ATO affects the crystallization behavior of PET. Isothermal crystallization kinetics are often limited to idealized conditions, in which parameters such as the temperature and pressure are constant. In practice, the external conditions change continuously, and this

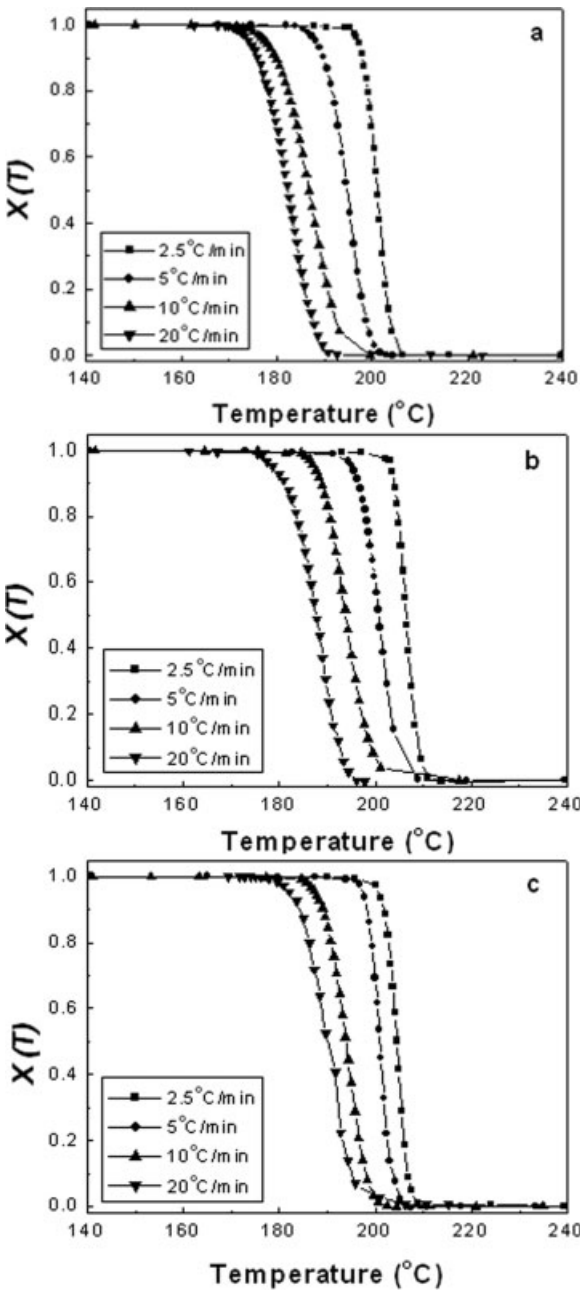

Figure 3 $X(T)$ as a function of temperature for the crystallization of PET and its ATO nanocomposites at four different cooling rates: (a) neat PET, (b) 99/1 PET/ATO, and (c) 95/5 PET/ATO.

makes the kinetics of crystallization dependent on instantaneous conditions.[24] The isothermal crystallization kinetics of polymers are usually analyzed in terms of the well-known Avrami equation:[25]

$$1 - X(t) = \exp(-Zt^n) \qquad (4)$$

where Z is a rate constant for the crystallization process and exponent n depends on the morphology of the growing crystalline regions and the nucleation process. This empirical equation has also been used

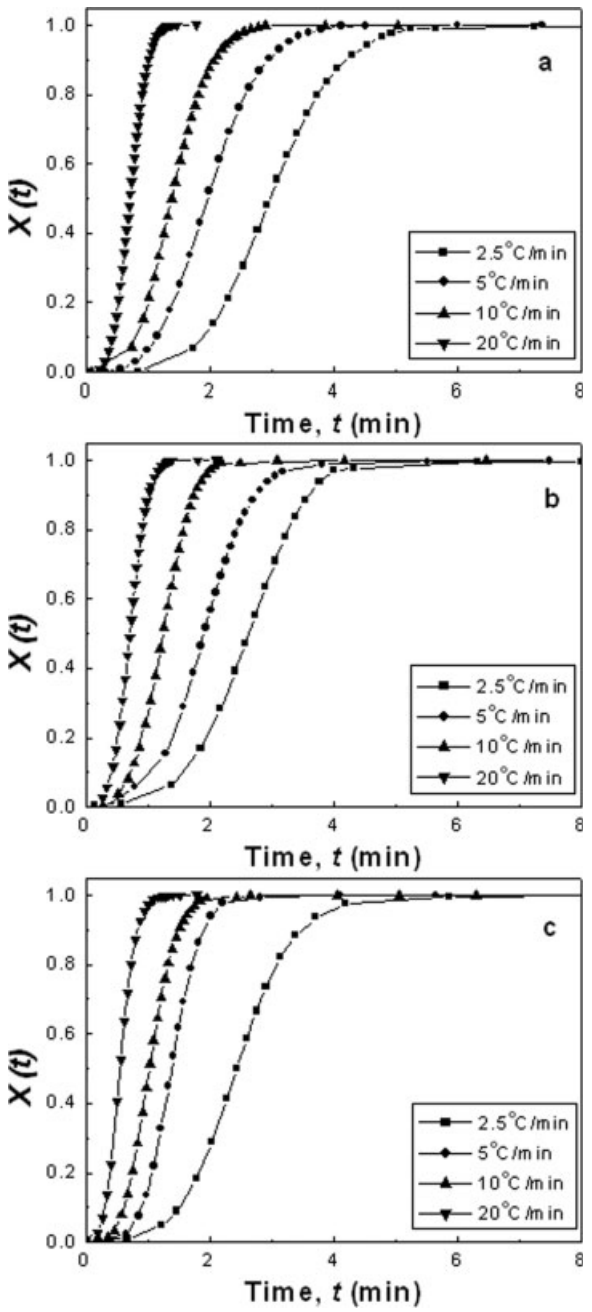

Figure 4 $X(t)$ as a function of time for the crystallization of PET and its ATO nanocomposites at four different cooling rates: (a) neat PET, (b) 99/1 PET/ATO, and (c) 95/5 PET/ATO.

to describe nonisothermal crystallization.[26,27] In this case, the parameters (n and Z) have different physical meanings because the temperature changes constantly during nonisothermal crystallization. However, the use of eq. (4) can still provide some insight into the kinetics of nonisothermal crystallization. The double logarithm of the Avrami equation gives the following relationship:

$$\log[-\ln(1 - X(t))] = \log Z + n \log t \tag{5}$$

Considering the nonisothermal character of the process investigated, Jeziorny[28] suggested that the value of rate parameter Z should be adequately corrected. The factor that should be considered is Φ. If we assume constant or approximately constant Φ, the final form of the parameter characterizing the kinetics of nonisothermal crystallization can be given as follows:

$$\log Z_c = \log Z/\Phi \tag{6}$$

Z_c is the correctional crystallization rate constant. Z_c in non-isothermal crystallization is obtained:

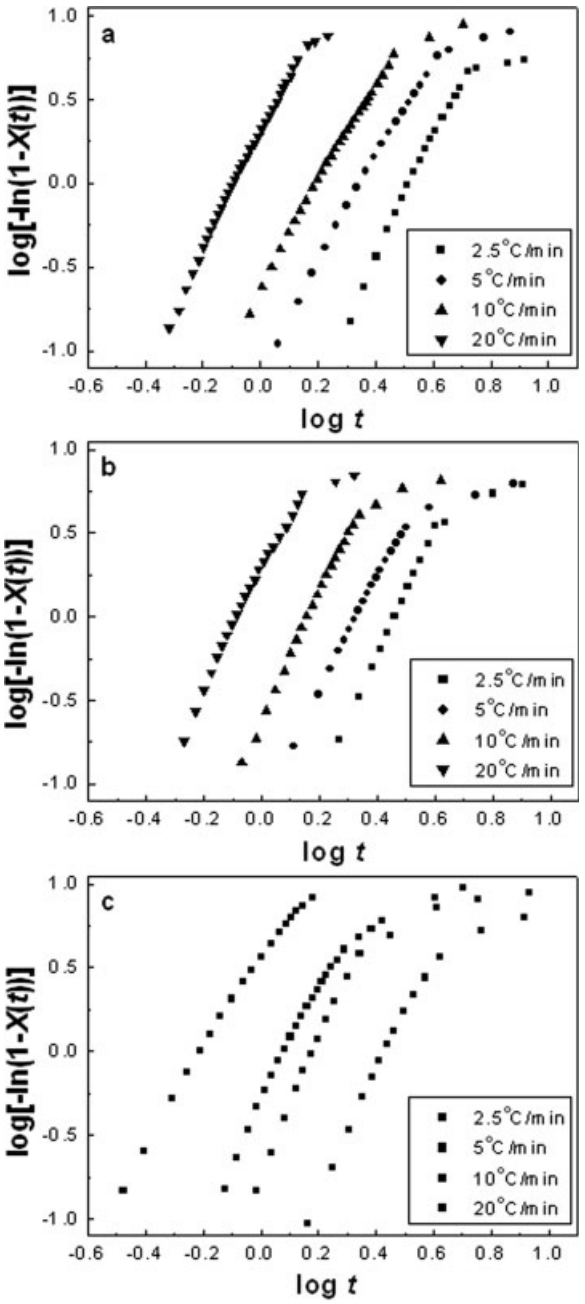

Figure 5 Plots of $\log\{-\ln[1 - X(t)]\}$ versus $\log t$ for the crystallization of (a) neat PET, (b) 99/1 PET/ATO, and (c) 95/5 PET/ATO at four different cooling rates.

TABLE III
Nonisothermal Crystallization Kinetic Parameters Based on the Avrami Equation Modified by Jeziorny

		Primary stage		Second stage	
Sample	Φ (°C/min)	n_1	Z_{c1}	n_2	Z_{c2}
Neat PET	2.5	3.61	0.17	0.27	1.55
	5	3.18	0.59	0.28	1.34
	10	3.07	0.87	—	—
	20	3.32	1.03	—	—
99/1 PET/ATO	2.5	3.82	0.20	0.38	1.42
	5	3.05	0.60	0.65	1.12
	10	3.74	0.87	0.67	1.10
	20	3.38	1.03	0.73	1.07
95/5 PET/ATO	2.5	3.83	0.221	0.59	1.23
	5	3.96	0.714	0.67	1.20
	10	3.33	0.93	0.72	1.14
	20	3.04	1.07	0.84	1.08

Figure 5 shows the double logarithmic plots of $\log\{-\ln[1 - X(t)]\}$ versus $\log t$ for neat PET and PET/ATO nanocomposites at various cooling rates. Consequently, a plot of $\log\{-\ln[1 - X(t)]\}$ versus $\log t$ would yield a straight line for each cooling rate. However, linear regression yields straight lines only in the early stages of crystallization, with a low degree of crystallinity (Fig. 5). Such a deviation of the Avrami plot in the later stage of crystallization was also found by Wang et al.[16] in the nonisothermal crystallization process of PET. Each region gives different values for n (n_1 and n_2) and Z_c (Z_{c1} and Z_{c2}; Table III). For the nonisothermal melt crystallization of neat PET, the average values were $n_1 = 3.30$ and $n_2 = 0.28$; for the 99/1 PET/ATO nanocomposite, the values were $n_1 = 3.51$ and $n_2 = 0.61$; and for the 95/5 PET/ATO nanocomposite, the values were $n_1 = 3.54$ and $n_2 = 0.71$. Obviously, the average values of n_1 for both the 99/1 PET/ATO nanocomposite and 95/5 PET/ATO nanocomposite were larger than those of neat PET, and this suggests that the nonisothermal crystallization of the PET/ATO nanocomposites corresponds to three-dimensional growth with heterogeneous nucleation. The value of Z_{c1} increased with the cooling rate increasing for both neat PET and the PET/ATO nanocomposites. However, the value of Z_{c2} decreased with the cooling rate increasing for both neat PET and the PET/ATO nanocomposites. The linear portions of each region were almost parallel to each other, and this suggests that the nucleation mechanism and crystal growth geometries were similar for the primary and secondary crystallization processes at all cooling rates. Therefore, the Avrami equation is invalid in the later stages (the so-called secondary crystallization) when deviation from linearity takes place.[29,30]

The secondary stage is generally considered the result of slower crystallization or crystal perfection, which is caused by spherulite impingement in the later stage of the crystallization process or by the further perfection or reorganization of initially poorly crystallized macromolecules or small and metastable crystals. If the secondary crystallization is not completed, the product will continue crystallizing in the course of use. This will lead to a continuous change in the properties of the product. Therefore, to obtain materials with stable and better properties, the nucleating agent is usually added in

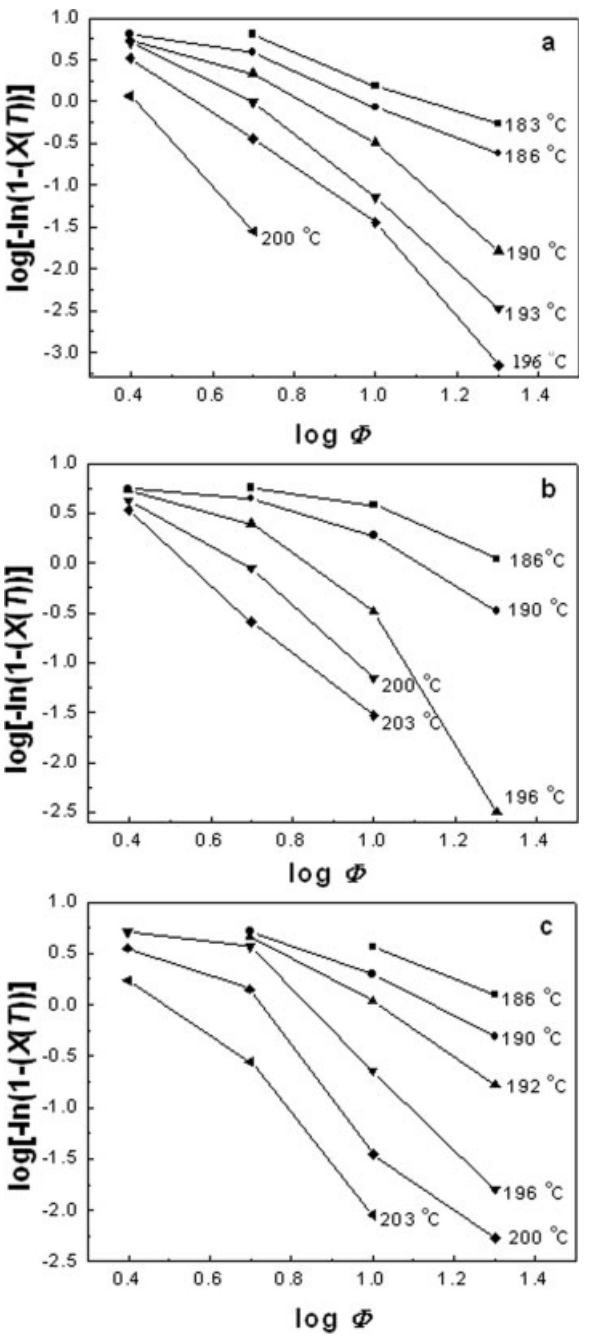

Figure 6 Ozawa plots of $\log\{-\ln[1 - X(T)]\}$ versus $\log \Phi$ for the crystallization of PET and its ATO nanocomposites at different temperatures: (a) neat PET, (b) 99/1 PET/ATO, and (c) 95/5 PET/ATO.

practical production and can accelerate secondary crystallization at the temperature of the maximum crystallization rate. Table II shows that ATO is an effective nucleating agent and does accelerate the crystallization rate of PET.

Because a cooling rate is necessary for the nonisothermal crystallization process, Ozawa[31] modified the Avrami equation by incorporating Φ:

$$1 - X(T) = \exp[-K(T)/\Phi^m] \quad (7)$$

where $K(T)$ is the cooling rate function and m is the Ozawa exponent. The double logarithm of the Ozawa equation gives the following relationship:

$$\log\{-\ln[1 - X(T)]\} = \log K(T) - m \log \Phi \quad (8)$$

Thus, a plot of $\log\{-\ln[1 - X(T)]\}$ versus $\log \Phi$ at a fixed temperature should yield a straight line. The parameters m and $K(T)$ can be determined from the slope and intercept of the line, respectively. Figure 6 shows the results for neat PET and PET/ATO nanocomposites according to the Ozawa method. It is clear that the linearity is questionable when varying over a large range. Thus, the Ozawa equation fails to describe the nonisothermal crystallization of ATO nanocomposites because the plots do not yield straight lines (as shown in Fig. 6). This can be tentatively explained as follows: at a given temperature, the crystallization processes at different cooling rates are at different stages; that is, the lower cooling rate is toward the end of the crystallization process, whereas for the higher cooling rate, the crystallization process is at an early stage. Figure 6 indicates that the Ozawa approach is not a suitable method for describing the nonisothermal crystallization process of neat PET and PET/ATO nanocomposites.

A new kinetic method proposed by Liu et al.[32] is also used to describe the nonisothermal crystallization of the PET/ATO nanocomposite. For the nonisothermal crystallization process, the relevant physical variables are $X(t)$, Φ, and T. By combining the Ozawa and Avrami equations, Liu et al. developed the following equation:

$$\log Z + n \log t = \log K(T) - m \log \Phi \quad (9)$$

This can be rearranged into

$$\log \Phi = \log F(T) - a \log t \quad (10)$$

where the kinetic parameter $F(T) = [K(T)/Z]^{1/m}$ refers to the value of the cooling rate that has to be chosen at the unit of crystallization time when the measured system amounts to a certain degree of crystallinity and a is the ratio of Avrami exponent n to Ozawa exponent m (i.e., $a = n/m$). According to eq. (10), the plots of $\log \Phi$ versus $\log t$ give a straight line for a given relative degree of crystallinity, as shown in Figure 7. All the values of the coefficient of correlation (R) are close to 0.99, indicating a good linear correlation; they are listed in Table IV. Thus, $\log F(T)$ and a can be obtained from the intercept and slope, respectively, and they are listed in Table IV. The values of $F(T)$ systematically increase with an increase in the relative crystallinity for the neat PET and two PET/ATO nanocomposites, indicating that

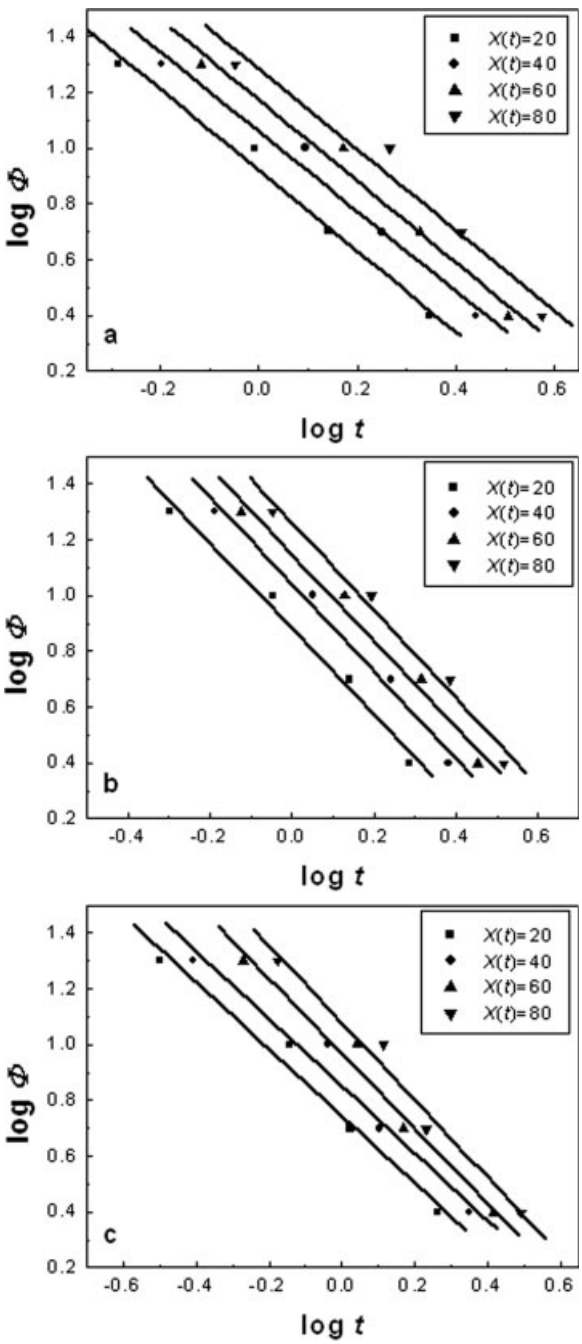

Figure 7 Plots of $\log \Phi$ versus $\log t$ for PET and its ATO nanocomposites with different crystallinities: (a) neat PET, (b) 99/1 PET/ATO, and (c) 95/5 PET/ATO.

at the unit of crystallization time, a higher cooling rate should be used to obtain a higher degree of relative crystallinity. The values of a are almost constant for each sample, being about 1.4 for neat PET, about 1.6 for the 99/1 PET/ATO nanocomposite, and about 1.2 for the 95/5 PET/ATO nanocomposite. It is clear that this combination method is successful in describing the nonisothermal crystallization process of neat PET and its ATO nanocomposites.

Considering the variation of T_p with the heating rate in differential thermal analysis, Kissinger[33] derived the activation energy (ΔE) in the following form:

$$\frac{d[\ln(\Phi/T_p^2)]}{d(1/T_p)} = -\frac{\Delta E}{R} \tag{11}$$

where R is the universal gas constant. Then, on the basis of the results in Table II, the slope of $\ln(\Phi/T_p{}^2)$ versus $1/T_p$ (Fig. 8) will give the crystallization activation energy, that is, $\Delta E = -R \times$ slope. According to the good linear relation, the ΔE values of nonisothermal crystallization were determined to be -205.3, -220.0, and -243.7 kJ/mol for neat PET and the 99/1 and 95/5 PET/ATO nanocomposites, respectively. ΔE is the activation energy required for transporting molecular segments to the crystallization surface. The higher the ΔE value is, the lower the crystallization ability is of the polymer. It is well known that the overall crystallization rate is the result of nucleation and growth rates. The nucleation rate of the PET/ATO nanocomposites was higher than that of the neat PET and increased with increasing ATO loadings because of the heterogeneous nucleation of ATO nanoparticles. However, the polymer chains in the nanocomposites exhibited lower diffusion rates because of the larger limiting viscosity number. Therefore, although the crystallization ability of the PET/ATO nanocomposite decreased in comparison with the neat PET, the crystallization rate of the PET/ATO nanocomposites was higher than that of the neat PET and increased with increasing ATO loadings.

TABLE IV
Nonisothermal Crystallization Kinetic Parameters of Various Samples with Different Values of $X(t)$ by the Combination of the Avrami and Ozawa Equations

		$X(t)$ (%)			
		20	40	60	80
Neat PET	$F(T)$	8.33	11.46	14.89	19.19
	a	1.45	1.43	1.46	1.44
	R	0.993	0.991	0.990	0.982
1/99 ATO/PET	$F(T)$	7.61	10.97	14.02	18.20
	a	1.53	1.56	1.55	1.57
	R	0.993	0.993	0.991	0.992
5/95 ATO/PET	$F(T)$	5.51	7.11	9.28	11.96
	a	1.20	1.21	1.34	1.39
	R	0.990	0.985	0.988	0.990

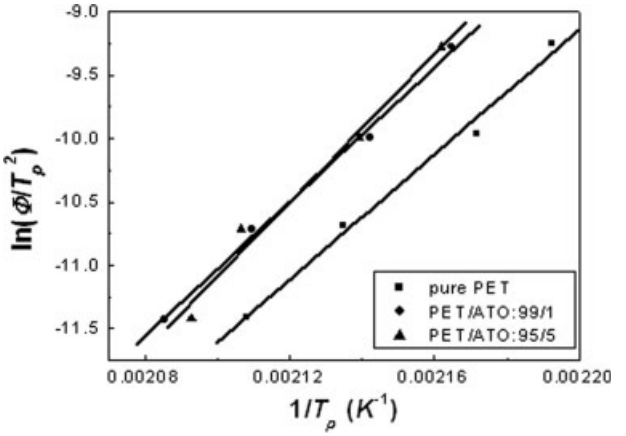

Figure 8 Determination of the activation energy describing the nonisothermal crystallization process for PET and its ATO nanocomposites based on the Kissinger method.

CONCLUSIONS

The PET/ATO nanocomposites were prepared via *in situ* polymerization. The applicability of several kinetic approaches for nonisothermal crystallization was examined. The kinetic analysis indicated that both the Avrami and Ozawa equations did not correlate satisfactorily with the experimental results. The Avrami analysis modified by Jeziorny indicated that the crystallization processes of PET and PET/ATO nanocomposites were distinctly divided into the primary and secondary crystallization stages, and the deviation of linearity at the longer time might be ascribed to the occurrence of the spherulite impingement in the secondary crystallization stage. After comparing different stages of crystallization at various cooling rates, the Ozawa analysis failed to provide an adequate description of the nonisothermal crystallization of neat PET and PET/ATO nanocomposites, probably because of the occurrence of secondary crystallization. A new kinetic method developed by Liu et al.[32] was successful in describing the nonisothermal crystallization process of PET/ATO nanocomposites. $t_{1/2}$ showed that the crystallization rate of PET and PET/ATO nanocomposites increased with increasing cooling rates, and the crystallization rate of PET/ATO nanocomposites was faster than that of neat PET at a given cooling rate because of the nucleation effect of ATO. In addition, the crystallization rate of PET/ATO nanocomposites increased with increasing ATO loadings. The ΔE values were calculated by the Kissinger method to be -205.3, -220.0, and -243.7 kJ/mol for the

neat PET and 99/1 PET/ATO and 95/5 PET/ATO nanocomposites, respectively.

References

1. Liu, L.; Qi, Z.; Zhu, X. J Appl Polym Sci 1999, 71, 1133.
2. Wang, Z.; Pinnavaia, T. J. Chem Mater 1998, 10, 3769.
3. Hu, Y.; Wang, S.; Ling, Z.; Zhuang, Y.; Chen, Z.; Fan, W. Macromol Mater Eng 2003, 288, 272.
4. Schmidt, D.; Shah, D.; Giannelis, E. P. Curr Opin Solid State Mater Sci 2002, 6, 205.
5. Yano, K.; Usuki, A.; Okada, A.; Kurauchi, T.; Kamigaito, O. J Polym Sci Part A: Polym Chem 1993, 31, 2493.
6. Messersmith, P. B.; Giannelis, E. P. J Polym Sci Part A: Polym Chem 1995, 33, 1047.
7. Chen, W.; Xu, Q.; Yuan, R. Z. Mater Sci Eng B 2000, 77, 15.
8. Chen, W.; Xu, Q.; Yuan, R. Z. Compos Sci Technol 2001, 61, 935.
9. Yoon, P. J.; Fornes, T. D.; Paul, D. R. Polymer 2002, 43, 6727.
10. Gao, G. Y.; An, S. L.; Yu, J. L.; Xiao, C. F. J Tianjin Polytech Univ 2005, 24, 12.
11. Huang, Y.; Li, Z. F.; Luo, G. H.; Wei, F.; Bu, J. L.; Li, A. Q. China Synth Fiber Ind 2004, 27, 1.
12. Rajpure, K. Y.; Kusumade, M. N.; Suallart, M. N. N.; Bhosale, C. H. Mater Chem Phys 2000, 64, 184.
13. Kim, K. H.; Lee, S. W.; Shin, D. W.; Park, C. G. J Am Ceram Soc 1994, 77, 915.
14. Orel, Z. C.; Orel, B.; Hodoscek, M.; Kaucic, V. J Mater Sci 1992, 27, 313.
15. Wu, Y.; Chi, Y. B.; Nie, J. X. J Funct Polym 2002, 15, 43.
16. Wang, Y. M.; Shen, C. Y.; Li, H. M.; Li, Q.; Chen, J. B. J Appl Polym Sci 2004, 91, 308.
17. Qin, C. Y.; Luo, M. F.; Gu, H. C.; Fang, T. N. J East China Univ Sci Technol 2001, 27, 261.
18. Chen, X. L.; Shao, W.; Li, C. Z. J East China Univ Sci Technol 2006, 32, 59.
19. Chen, X. L.; Li, C. Z.; Shao, W.; Du, H. L.; Burnell-Gray, J. S. J Appl Polym Sci 2007, 105, 1490.
20. Qiu, G.; Tang, Z. L.; Huang, N. X.; Gerking, L. J Appl Polym Sci 1998, 69, 729.
21. Ma, Y.; Agarwal, U. S.; Sikkema, D. J.; Lemstra, P. J. Polymer 2003, 44, 4085.
22. Jong, S. C. T.; Bao, S. P. J Polym Sci Part B: Polym Phys 2004, 42, 2878.
23. Cebe, P.; Hong, S. D. Polymer 1986, 27, 1183.
24. Di Lorenzo, M. L.; Silvestre, C. Prog Polym Sci 1999, 24, 917.
25. Avrami, M. J. Chem Phys 1939, 7, 1130.
26. Suphaphol, P. J Appl Polym Sci 2000, 78, 338.
27. Xu, W.; Liang, G.; Wang, W.; Tang, S.; He, P.; Pan, W. P. J Appl Polym Sci 2003, 88, 3093.
28. Jeziorny, A. Polymer 1978, 19, 1142.
29. Hay, J. N.; Mills, P. J. Polymer 1982, 23, 1380.
30. Hay, J. N.; Perzekop, Z. J. J Polym Sci Polym Phys Ed 1978, 16, 81.
31. Ozawa, T. Polymer 1971, 12, 150.
32. Liu, T. X.; Mo, Z. S.; Wang, S. E.; Zhang, H. F. Polym Eng Sci 1997, 37, 568.
33. Kissinger, H. E. J Res Natl Stand 1956, 57, 217.